ACSNANO

www.acsnano.org

ARTICLE

Bioorthogonal Catalysis for Treatment of Solid Tumors Using Thermostable, Self-Assembling, Single Enzyme Nanoparticles and Natural Product Conversion with Indole-3-acetic Acid

Samira Sadeghi,[■] Nihar D. Masurkar,[■] Girish Vallerinteavide Mavelli, Siddharth Deshpande, Warren Kok Yong Tan, Sherman Yee, Shin-Ae Kang, Yoon-Pin Lim, Edward Kai-Hua Chow, and Chester L. Drum*

Cite This: *ACS Nano* 2022, 16, 10292–10301

Read Online

ACCESS | Metrics & More | Article Recommendations | Supporting Information

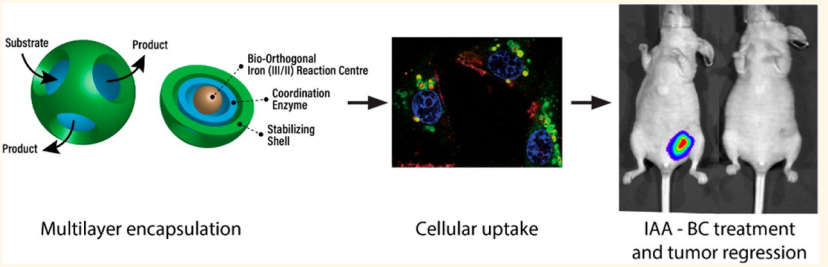

ABSTRACT: **Bioorthogonal catalysis (BC) generates chemical reactions not present in normal physiology for the purpose of disease treatment. Because BC catalytically produces the desired therapy only at the site of disease, it holds the promise of site-specific treatment with little or no systemic exposure or side effects. Transition metals are typically used as catalytic centers in BC; however, solubility and substrate specificity typically necessitate a coordinating enzyme and/or stabilizing superstructure for *in vivo* application. We report the use of self-assembling, porous exoshells (tESs) to encapsulate and deliver an iron-containing reaction center for the treatment of breast cancer. The catalytic center is paired with indole-3-acetic acid (IAA), a natural product found in edible plants, which undergoes oxidative decarboxylation, via reduction of iron(III) to iron(II), to produce free radicals and bioactive metabolites. The tES encapsulation is critical for endocytic uptake of BC reaction centers and, when followed by administration of IAA, results in apoptosis of MDA-MB-231 triple negative cancer cells and complete regression of *in vivo* orthotopic xenograft tumors ($p < 0.001$, $n = 8$ per group). When Renilla luciferase (rLuc) is substituted for horseradish peroxidase (HRP), whole animal luminometry can be used to monitor *in vivo* activity.**

KEYWORDS: *thermostable, exoshell, protein encapsulation, bioorthogonal catalysis, tumor regression*

Current treatment regimens for cancer are often toxic and carry the burden of dose limiting systemic side effects.[1,2] Bioorthogonal catalysis (BC) is a new approach that provides *in situ* catalytic production of an active agent, thus focusing treatment on the site of disease with minimal systemic exposure. BC catalytic centers often rely on transition metals, which readily undergo changes in oxidation state at potentials conducive for *in vivo* catalytic reactions due to their partially filled d subshell orbitals. For this reason, metals such as iron, ruthenium, palladium, and copper provide promising substrates for BC focused chemistries that are unrelated, or "orthogonal", to the surrounding physiology.[3]

Iron is one of the best studied transition metals and can adopt multiple oxidation states with iron(II) and iron(III), the ferrous and ferric forms being the most common. Iron has well-known biocompatibility and is present in both endogenous and exogenous enzymes with highly specific substrate

Received: December 28, 2021
Accepted: April 29, 2022
Published: June 2, 2022

https://doi.org/10.1021/acsnano.1c11560
ACS Nano 2022, 16, 10292–10301

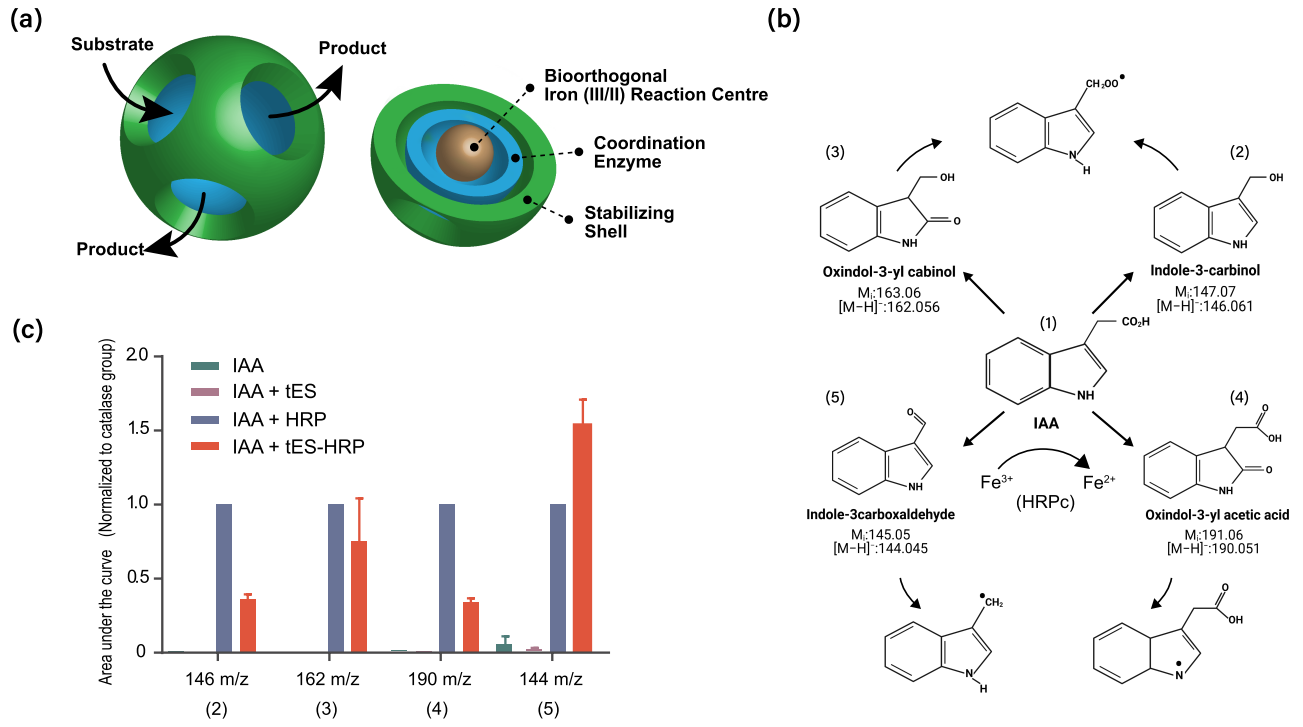

Figure 1. (a) Schematic representation of an assembled tES shell with surface pores for entry and exit of bioorthogonal catalysis substrates and products (left) and multilayer approach to bioorthogonal catalytic center cutaway (right). (b) Chemical products of IAA and their free radical derivatives. (c) Mass spectrometry of IAA products demonstrating catalytic specificity of tES-HRP.

specificities.[4] Peroxidase enzymes like horseradish peroxidase (HRP) have several features suitable for BC, including the ability to align the π-orbital of elemental iron with paired substrates using a heme prosthetic group.[5] Although peroxidases have been extensively studied *in vitro*, their use in BC for treating solid tumors has been limited due to issues of cellular delivery and *in vivo* protein stability.[6] Unlike mammalian peroxidases, HRP does not require hydrogen peroxide to oxidize its substrate and exhibits an optimal catalytic activity at low pH (6.0−6.5) characteristic of tumor microenvironments.[7−10] Because HRP is active under low oxygen tensions, it may be well-suited for targeting hypoxic regions of tumors.[11]

Substrates compatible with BC treatment regimes vary widely and include both prodrugs and natural products that are converted either to therapeutics or to organelle-specific probes.[12−14] For the treatment of solid tumors, a BC substrate would optimally have a near zero profile of systemic side effects and, when converted by an *in situ* catalyst, have high potency localized treatment effect. Indole-3-acetic acid (IAA) is a component of edible plants and a member of the auxin class of molecules that regulate plant growth and stress response. IAA can undergo one electron oxidation, initiated by decarboxylation, in response to the reduction of an iron catalyst from iron(III) to iron(II).[11] This reaction generates biologically active intermediates and free radicals that induce oxidative degradation and apoptosis of target cells. IAA is also a poor substrate for mammalian peroxidases and has undergone dose response human trials with a highly favorable safety profile.[11,15,16] Further, past attempts at site-specific IAA conversion using either gene-directed or antibody-directed methodologies have met with severe limitations including poor cellular expression of transformed enzymes and rapid physiological clearance.[17,18]

Enzyme encapsulation with a single or double stoichiometric ratio is a recent approach to the stabilization and delivery of catalytic moieties. To test the effect of nanoencapsulation on suitability for *in vivo* BC, we used a 12 nm thermostable "exoshell", tES.[19,20] tESs are highly thermostable (up to 92.5 °C), can encapsulate and stabilize single enzymes, and have four 4.5 nm pores which allow diffusional exchange of substrate and product with an internalized catalyst (Figure 1a). tESs protect proteins from proteolysis,[19] act as an artificial chaperone to fold proteins,[21] and stabilize proteins when used as a lyoprotectant.[22] Cellular and *in vivo* applications of tESs, however, have not been characterized.

We describe the use of tES-HRP stabilized iron(III) as a multilayered catalytic center for BC to treat an *in vivo* model of breast cancer. The therapeutic strategy couples the reactive center with a benign natural product substrate, normally consumed in low quantities in everyday diets, thus offering a promising approach to the clinical application of BC.

RESULT AND DISCUSSION

tES Is a Highly Stable Engineered Shell That Encapsulates Proteins. In this study, we hypothesize that single and/or double enzyme nanoencapsulation will simultaneously enable stabilization, cellular delivery, preservation of substrate entry and allowance for egress of the bioorthogonal product. tESs contain an 8 nm aqueous center (Figure 1a) and mutational variants of tESs create net positive (tES(+)), negative (tES(−)), and neutral (tES(±)) interior charge environments.[19] A phenylalanine to histidine mutation at position 116 (tES(+)F116H) (Figure S1) results in tESs that disassemble at pH 5.8 and reassemble at pH 8.0 (Figure S2a). The expression and purification of tES-rLuc (rLuc encapsulated within tES(+)F116H) and tES(+)F116H were performed as previously described[19] (Figure S1, Figure S2b-i).

https://doi.org/10.1021/acsnano.1c11560
ACS Nano 2022, 16, 10292−10301

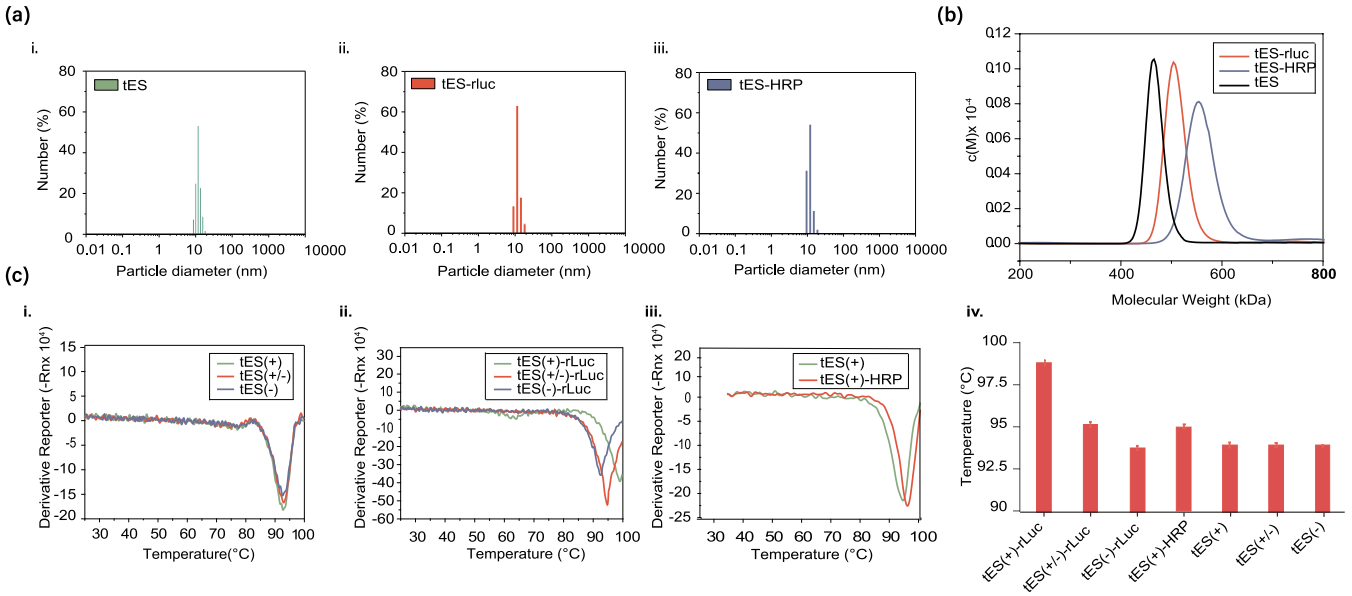

Figure 2. (a) Dynamic light scattering (DLS) of tES, tES-rLuc, and tES-HRP with a measured hydrodynamic diameter of ∼12 nm. (b) Mass-based size distribution of tES, tES-rluc, and tES-HRP calculated from analytical ultracentrifugation (AUC) demonstrating that tES encapsulates a single rluc molecule (36 kDa) and one or two HRP molecules (44 kDa). (c) Differential scanning fluorometry (DSF) analysis of tES-rluc. Encapsulation of rluc within tES(+) resulted in a ∼6 °C increase in the thermostability of tESs. DSF demonstrated a significant, but smaller, effect for HRP on shell stability. In (a)−(c), data are shown as mean ± SEM, n = 3.

We previously demonstrated tESs can increase the soluble and functional expression of recombinant proteins covalently fused within the tES interior.[19] To create a platform for noncovalent encapsulation, we developed a protocol to internalize macromolecules within the tES volume using charge−charge complementarity. For HRP (pI 5.6) encapsulation, tES(+)F116H was mixed with a 10-fold molar excess of free HRP at pH 5.8 followed by pH adjustments to 8.0 and subsequent purification using size-exclusion chromatography (SEC) to form tES-HRP (Figure 1a). The enzymatic activity of encapsulated HRP was confirmed with 3,3′,5,5′-tetramethylbenzidine (TMB) substrate (Figure S2b-ii, brown absorbance overlaid on SEC profile).

Despite Strong Physicochemical Effects, Internalized Enzymes Access Substrates. We hypothesized that, whereas the tESs surround and stabilize an encapsulated reaction center, BC could occur via the triangular pores allowing entrance of IAA substrate and egress of IAA products. To test whether tES-HRP can metabolize IAA with a comparable rate and product distribution to free HRP, we incubated tES, free HRP, and tES-HRP (1 μM final concentration for each) with 2.5 mM IAA at 37 °C for 1 h. The products of the IAA-HRP reaction (Figure S3) were analyzed with ultrahigh performance liquid chromatography followed by time-of-flight mass spectrometry (UPLC-QTOF). As shown in Figure S4, the retention times and mass spectra m/z were the same for free HRP and tES-HRP with a qualitatively similar pattern of abundance. Measurements were standardized to an indole-3-carboxaldehyde commercial standard (Figure S5). A 23% decrease in area under the curve for total ion count (retention time 5.5−11.6 min) was observed between free HRP and tES-HRP, suggesting that the specific activity of encapsulated HRP was marginally lower. Although all products of IAA could be identified (Figure 1b), encapsulation by tESs appears to result in a catalytic preference for the indole-3-carboxaldehyde product (Figure 1c). We hypothesize that nanoencapsulated HRP may undergo changes to the electrostatic, steric, diffusional, or redox environment, which effects the distribution of enzyme products.[21]

We then confirmed the uniformity of postencapsulation assembly of tESs by dynamic light scattering (DLS). Similar to tES, tES-rLuc and tES-HRP assemblies were found to be monodisperse with a diffusional diameter of 12 nm (Figure 2a). Transmission electron microscopy (TEM) confirmed a spherical morphology and uniform size distribution for all the three particle types (Figure S2c). In TEM imaging of pH 5.8, we were unable to visualize tES spheres, the tES subunits, or encapsulated enzymes, likely due to limits of TEM resolution.

tES Encapsulates Either One or Two HRP Molecules or One Luciferase Molecule per Shell. Using analytical ultracentrifugation (AUC), we measured the encapsulation efficiency of macromolecules inside tES.[23,24] Sedimentation velocities were compared among tES, tES-rLuc, and tES-HRP at 40000g and 20 °C. The observed molecular weight of tES was 466 kDa, whereas that of tES-HRP was 554 kDa (Figure 2b), consistent with the calculated molecular mass of tES (466 kDa) plus two HRP molecules (∼44 kDa, each). The molecular weight of tES-rLuc was 502 kDa, consistent with each tES encapsulating a single molecule of rLuc (36 kDa). On the basis of its ∼3 nm Stokes radius,[25] one or two HRP monomers can be accommodated within the tES internal volume. Of note, this represents a 120 mM concentration (or 30% v/v) of HRP in the 2.7 × 10^{-23} L shell volume and a ∼200-fold concentrating effect compared with the 500 μM loading concentration of HRP. This suggests a strong role for enthalpic forces that overcome the entropic cost of encapsulation. The variation in encapsulation efficiency between HRP and rLuc may also be due to different methods of substrate encapsulation (Figure S1). Likewise, a broadening of the tES-HRP profile (Figure 2b) was consistent with a population of both singly and doubly encapsulated HRP

https://doi.org/10.1021/acsnano.1c11560
ACS Nano 2022, 16, 10292−10301

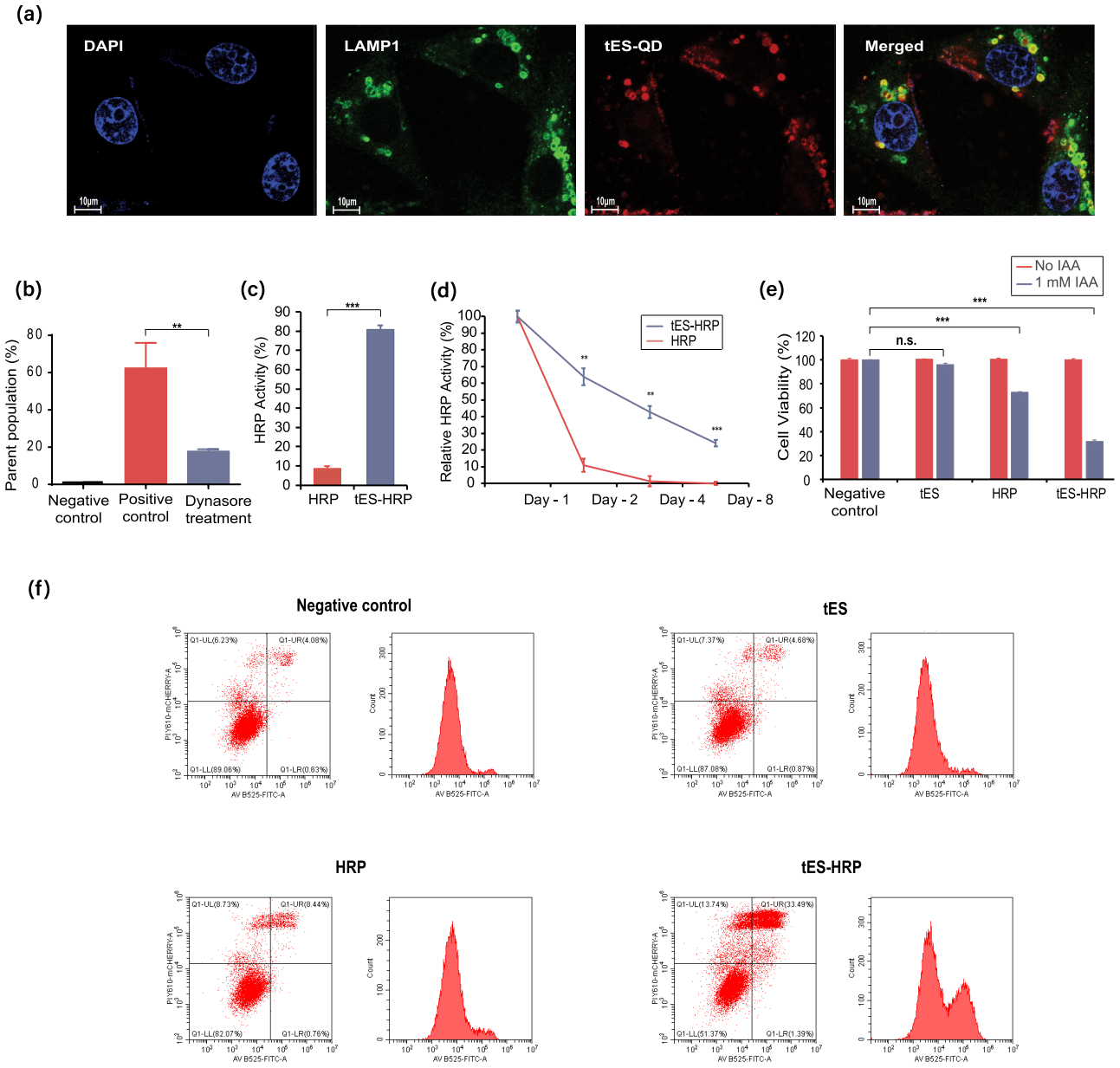

Figure 3. (a) Co-localization of tES-QDs within the lysosomes was analyzed by confocal microscopy of MDA-MB-231 cells incubated with tES-QDs. The scale bar is 10 μm. The nucleus is stained with DAPI and lysosomes by LAMP1. (b) Pretreated MDA-MB-231 cells with Dynasore exhibited 67% reduction ($P < 0.005$) in the uptake of tES, suggesting an endocytic pathway. (c) Incubation of tES-HRP or free HRP in Artificial Lysosome Fluid (ALF) for 2 h displayed significant protection to the tES-encapsulated HRP compared to the free enzyme. (d) tES maintained 30% of HRP activity upon 8 day incubation with serum proteases, although negligible activity was observed with free HRP. (e) MDA-MB-231 cells treated with tES-HRP followed by indole-3-acetic acid (IAA) incubation exhibited 70% reduction in cell viability compared to the 30% shown by free HRP. (f) Apoptosis assay using Annexin V-FITC/propidium iodide double staining in MDA-MB-231 cells were analyzed by flow cytometry. In (a)−(f), data are shown as mean ± SEM, $n = 3$. *** $P < 0.001$, ** $P < 0.01$.

molecules, which is in accordance with densitometric analysis.[22]

tES Assembly Is Mutually Stabilized via Encapsulation. The biological activity of encapsulated enzymes is dependent on the retention of a precise and complex three-dimensional structure. Therefore, the thermodynamic and biochemical stability of tES and tES-encapsulated reaction centers in the cellular environment is critical. As rLuc is thermolabile, we evaluated the stabilizing effect of tES with a thermal shift assay. This assay monitors a test protein using a thermofluor that binds to exposed hydrophobic residues and changes the fluorescent signal as the protein denatures.[26] Although tESs were stable up to 92 °C (Figure 2c), the encapsulation of rLuc (which has a net negative charge at pH 7.5) within tES(+)F116H resulted in an increase in the thermostability of tES up to 98 °C. The stability of the exoshell was unaffected upon encapsulation of rLuc within tES(−)-F116H, consistent with a charge−charge complementation mechanism for stabilization. HRP was measured in the tES(+)F116H shell and demonstrated a significant, but smaller, effect on shell stability.

tES Undergoes Endocytosis-Mediated Cellular Uptake and Stabilizes Encapsulated Reaction Centers. Confocal microscopic analyses confirmed the cellular uptake of

https://doi.org/10.1021/acsnano.1c11560
ACS Nano 2022, 16, 10292−10301

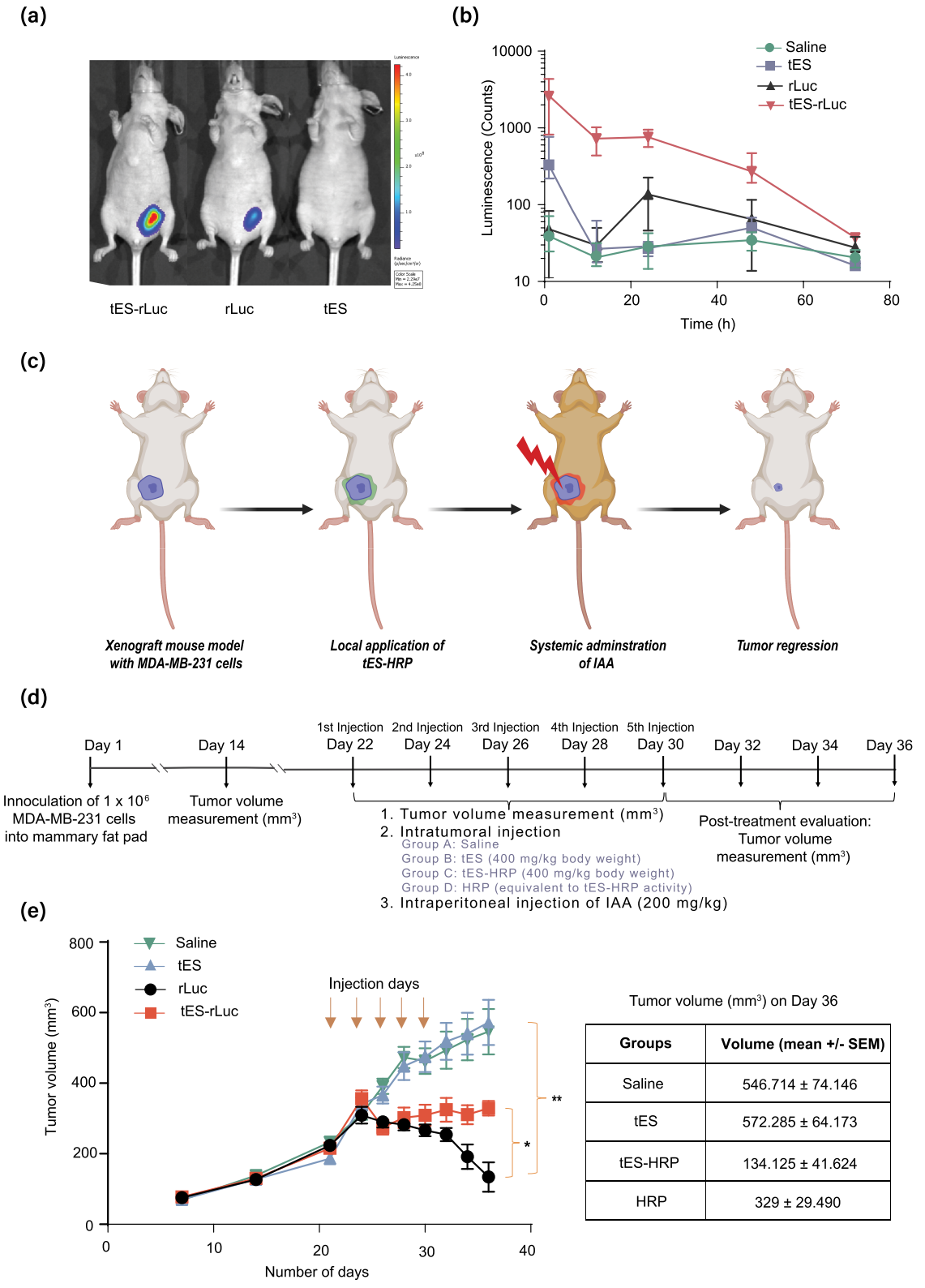

Tumor volume (mm³) on Day 36

Groups	Volume (mean +/- SEM)
Saline	546.714 ± 74.146
tES	572.285 ± 64.173
tES-HRP	134.125 ± 41.624
HRP	329 ± 29.490

Figure 4. (a,b) Bioluminescence emitted from mice injected with tES-rLuc/r-Luc revealed the clearance of tES-rLuc with a transient decrease in luminescence. The clearance of tES is studied through an intratumoral injection of tES-rLuc, followed by an intraperitoneal injection of coelenterazine substrate at 0, 1, 12, 24, 48, and 72 h. The luminescence showed a negligible signal after 72 h (the experiment was performed with three mice per group). (c) Schematic representation of enzyme-prodrug therapy is shown. (d) Treatment protocol for the *in vivo* enzyme-prodrug therapy is shown. (e) Mice were administrated intratumorally with saline, tES, HRP, or tES-HRP followed by an intraperitoneal injection of the prodrug IAA every other day (a total of five injections). Error bars indicate mean ± standard error of the mean (n = 8 per group). No deaths occurred in the tES-HRP group, which showed a complete regression in tumor volume. Data are shown as mean ± SEM ** $P < 0.01$, * $P < 0.05$.

https://doi.org/10.1021/acsnano.1c11560
ACS Nano 2022, 16, 10292−10301

tES shells. The shells were encapsulated with quantum dots (QDs) and the 24 h post-transfection images revealed the colocalization of tES-QDs in lysosomes of the triple negative breast cancer cell line, MDA-MB-231 (Figure 3a). This was further confirmed by using the commercial endocytosis inhibitor, Dynasore. In comparison with the case for positive controls, pretreatment with Dynasore induced a 67% reduction ($P < 0.005$) in the uptake of tES (Figure 3b and Figure S6), suggesting the endosomal trafficking of tES. Given the successful cellular uptake of tES, we then examined the potential toxicity of tES using CTG assay. Cellular uptake of tES resulted in negligible cell death at 8 and 24 h postincubation, reflecting the nontoxicity of these nanoparticles (Figure S7). To determine the enzyme activities in the degradative environment of lysosomes, we tested the stability of encapsulated HRP/rLuc activity in reconstituted Artificial Lysosome Fluid (ALF) using the technique of Stopford et al.[27] tES-HRP and HRP were incubated with ALF for 2h at 37 °C followed by assay of enzyme activity. tES protected the encapsulated HRP compared to loss of activity of the free enzyme (Figure 3c). At both ratios evaluated, tES stabilized HRP activity by 10−70 fold. Similar results were observed when tES-rLuc was incubated with ALF (Figure S8). The stability of tES-HRP on exposure to serum proteases was evaluated. tES-HRP demonstrated 60% higher activity compared to that of free HRP after 2 days of incubation (Figure 3d). By day 8, ∼30% activity of the encapsulated HRP was retained compared to negligible activity for free HRP.

tES-HRP and IAA Characterization for BC. Bioorthogonal catalysis offers highly controlled and localized generation of therapeutics and circumvents issues associated with the delivery and distribution of drug molecules and minimizes their side-effects on healthy tissues.[28−31] We hypothesized that tES-HRP could be applied to BC to selectively activate IAA at the site of a solid tumor.[32−34] IAA is a natural product with low toxicity and very low rates of nonspecific activation in humans, even when administered in high doses of more than 100 mg/kg body weight and is thus generally regarded as safe from a regulatory standpoint.[11,15,35] IAA undergoes one-electron oxidation in the presence of HRP to form carbon-centered free radicals such as indol-3-yl, skatolyl, 3-methylene-2-oxindole, and oxindol-3-yl radicals.[36−38] These reactive products cause DNA, lipid, and protein oxidation, resulting in cellular cytotoxicity and apoptosis.[18,36,38] We investigated the effects of HRP/IAA on MDA-MB-231 and BT549 cell lines. In both cell lines, upon incubation of tES-HRP transfected cells with IAA (Figure 3e, Figure S9), the cell viability decreased by 50−70% compared to 0−25% cell death observed with free HRP ($P < 0.01$ vs free IAA and tES group and $P < 0.05$ vs free HRP group). Further, the induction of apoptosis due to cytotoxicity was demonstrated via double staining with Annexin V-FITC and propidium iodide in flow cytometry analysis (Figure 3f).

***In Vivo* Biodistribution and Clearance Studies.** The biodistribution of tES was evaluated in athymic nude mice using a bioluminescent reporter protein, rLuc. Mice were intratumorally injected with tES-rLuc/saline followed by intraperitoneal (i.p.) injection of rLuc substrate at 1 and 3 h before IVIS analysis. After 1 h, tES accumulated mainly in the tumor, whereas after 3 h, it could be detected in the intestine as well (Figure S10). Additionally, the IVIS imaging revealed the clearance of tES-rLuc activity with a transient increase in hepatic luminescence, suggesting functional rLuc survival outside the area of injection. By 72 h, no bioluminescence signal could be detected (Figure 4a,b and Figure S11). In our study, we observed the encapsulated rLuc remained stable ($t_{1/2}$ = ∼10 h) until the complete elimination of tES, consistent with the ability of stabilized exoshells to protect the activity of an internalized enzyme *in vivo*. Likewise, the low activity of free rLuc observed in the peritumoral environment suggests a potential use of tES-rLuc in bioluminescence imaging.

tES Is Nontoxic at the Tested Dose. A toxicity study was performed by intratumorally injecting tES(+) (400 mg·kg^{-1}) to breast tumor-bearing mice for 5 consecutive days (Figure S12), followed by the evaluation of blood biochemistry. No toxicity was observed in markers of liver or renal injury (albumin, alkaline phosphatase, alanine aminotransferase, total bilirubin, creatinine, total protein, and blood urea nitrogen), and hematology values remained within normal limits (WBC, RBC, hemoglobin, and hematocrit levels) (Figure S12).

tES plus HRP Induces Tumor Regression with Systemic Administration of IAA Substrate. The effect of tES-encapsulated HRP and IAA treatment on tumor regression was evaluated in a triple negative breast cancer xenograft mouse model (Figure 4c). CrTac:NCr-Foxn1nu mice (n = 8 per group) were injected with MDA-MB-231 cells into the mammary fat pad. When the tumor reached an approximate size of 200−250 mm^3, the mice were intratumorally administered with saline, empty tES (400 mg·kg-1 body weight), tES-HRP (400 mg·kg-1 body weight), or free HRP (equivalent to the activity of 400 mg·kg^{-1} body weight of tES-HRP) followed by an i.p. injection of the prodrug IAA (200 mg·kg^{-1} body weight) every other day for five times (Figure 4d). A dose of 200 mg/kg of IAA was chosen on the basis of prior toxicity and tolerability studies,[18,39] and animals were monitored both on a daily basis and via biomarkers and histology after sacrifice for any signs of toxic effects. Intratumoral delivery, either as a primary treatment or as a neoadjuvant/postresection strategy to prevent tumor recurrence, is an emerging alternative to conventional therapies and i.p. administration is an established methodology to substitute for intravenous administration in mice tumor models.[40−43]

Tumor volumes reached an average maximum size of 550−600 mm^3 in control mice treated with either saline or tES (Figure 4e). The tumor growth halted in mice receiving free HRP and IAA during the treatment regimen of 5 days; however, the tumor continued to grow thereafter and two mice in this control arm died before the study ended. Five cumulative deaths (one, two, and two mice from saline, tES(+), and free HRP groups, respectively) occurred in the control groups before study termination. No deaths occurred in the experimental arm, i.e., the tES-HRP group, which showed a complete regression in tumor volume (Figure 4e, *P < 0.05; **P < 0.01). The body weights of the mice from the different treatment groups exhibited no weight loss, likewise consistent with the absence of severe side effects[31] (Figure S13). Tissues from mice treated with saline, tES, and free HRP stained negative for cleaved caspase-3, an enzyme involved in the activation of intrinsic and extrinsic apoptotic pathways.[44] In contrast, tES-HRP-treated mice showed cleaved caspase-3 activation (Figure S14), consistent with the mechanism of action for IAA-mediated induction of apoptosis.[18,36,38] We also note that, although we did not perform a formal dose finding study, an earlier experiment performed at 100 mg·kg^{-1} body weight showed tumor growth suppression; however, no regression (Figure S15). This earlier experiment did inform

https://doi.org/10.1021/acsnano.1c11560
ACS Nano 2022, 16, 10292−10301

the design of the reported results and does suggest a trend for tumor response and increase of IAA dose. Likewise, although tES-HRP showed no increase in markers of toxicity, a caveat of our study is the CrTac:NCr-Foxn1nu (nude) mouse model and is likely not reflective of risk in an immunocompetent organism. A caveat of our study, in consideration of clinical translation, will be predicting the clinical doses of the tES-HRP depot and systemic IAA. Overall, we demonstrate an effect specific to tES-enabled BC as tumor growth quickly resumed after the fifth injection period for both controls and HRP administered without tES encapsulation. In contrast, mice injected with tES-HRP continued tumor volume regression significantly after the fourth injection of IAA to a near undetectable level. Thus, taken together, our data are consistent with tES as an enabling technology for BC.

CONCLUSION

The therapeutic application of bioorthogonal catalysis represents a special challenge, requiring biocompatible, physicochemically stabile catalytic reaction centers. Herein, we demonstrate the specific effect of reaction centre encapsulation using thermostable exoshells. Because the catalytic substrate, IAA, is a well characterized and ubiquitous nutritional component, the described system may be useful for low toxicity treatment of solid tumours. The general approach of thermostable encapsulation may likewise be helpful in further applications of *in vivo* stabilized, bioorthogonal catalysis.

METHODS

Preparation of tES-HRP Nanoparticles. The gene construct for tES was described previously[19] (Figure S1). The plasmid carrying tES gene was transformed into chemically competent XL1 Blue *Escherichia coli* cells and cultured on Luria−Bertani (LB) agar (Axil Scientific, USA) plates with kanamycin (25 $\mu g \cdot mL^{-1}$; ThermoFisher, Singapore); the positive colonies were confirmed by sequencing. A single positive colony was inoculated in LB broth (100 mL) supplemented with kanamycin (50 $\mu g \cdot mL^{-1}$). Following overnight incubation at 37 °C, the starter culture (12.5 mL) was used to inoculate LB broth (500 mL). The culture was allowed to grow until an absorbance (OD600) of 0.4 was attained. Protein expression was induced with the addition of isopropyl β-D-1-thiogalactopyranoside (IPTG, 0.4 mM; Axil Scientific) and continued for 4 h at 37 °C. The cells were pelleted by centrifugation at 13750*g* for 10 min. The cell pellet was resuspended in a lysis buffer (50 mM Tris−HCl, pH 8.0, 200 mM NaCl, and 0.1% Triton-X 100), and the suspension was sonicated and centrifuged. The supernatant was purified with a two-step chromatography procedure, including hydrophobic interaction chromatography (HIC) using HiPrep Phenyl FF (low sub) 16/10 (GE Healthcare) and SEC using a Superdex S-200 10/300 GL column (GE Healthcare). The buffers used were as follows: HIC buffer A, 25 mM Tris−HCl, 150 mM NaCl, 1 M $(NH_4)_2SO_4$, pH 8.0; HIC buffer B, 25 mM Tris−HCl, 150 mM NaCl, pH 8.0; SEC buffer, 1× phosphate-buffered saline (PBS), pH 8.0. The purity of the SEC fraction was analyzed using sodium dodecyl sulfate polyacrylamide gel electrophoresis (SDS-PAGE). The SEC fraction was acidified for shell disassembly and the sample was subjected to SEC with 50 mM Tris−citrate buffer, pH 5.8. The disassembled tES subunits were collected and mixed with a 10-fold molar excess of HRP (Sigma, CA, USA), and the mixture was incubated at 4 °C for 30 min. The pH of the mixture was raised to 8.0, and the assembled tES encapsulating HRP (tES-HRP) was separated from free HRP using SEC.

Preparation of tES-rLuc Nanoparticles. The cloning, expression, and purification of tES-rLuc were performed as previously reported[19] (Figure S1). The expressed protein was used for *in vitro* and *in vivo* studies.

Characterization of nanoparticles. The particle sizes of tES, tES-rLuc, and tES-HRP were measured by DLS (Nanobrook Omni, Brookhaven). The prepared tES proteins were placed in disposable sized cuvettes, and the measurements were performed at a scattering angle of 90° at room temperature. The morphologies of all the tES proteins were studied using TEM (JEOL JEM-1220 TEM).

Thermal Shift Assay. All thermal shift assays were performed with an Applied Biosystems Protein Thermal Shift Starter Kit (Cat. No. 4462263). Replicates containing 1 μM tES/tES-rLuc in 1× PBS were mixed with a 1× dye provided in the kit. Reactions were carried out in 384-well PCR plates (Thermo Scientific), which were sealed with adhesive sealing sheets (AB-0558, Thermo Scientific). The plates were analyzed on an Applied ViiA 7 Real-Time PCR system at temperatures ranging from 25 to 99.9 °C at a ramp rate of 0.05 °C·s^{-1}.

Encapsulation Efficiency Determination. A Beckman Coulter ProteomeLab XL-I analytical ultracentrifuge was employed for the AUC analysis of tES, tES-rLuc, and tES-HRP. Each sample (1 μM) was suspended in PBS and loaded into one of the two holes of an Epon cell equipped with sapphire windows. The other hole was loaded with PBS only. These cells were housed in a four-hole rotor (Ti-60, Beckman-Coulter). The optical densities of the samples at 280 nm were measured as a function of time at a constant rotation speed of 40000*g* at 20 °C. The experiment typically continued for 7−8 h until predominantly all the particles had sedimented to the bottom of the cells. Data were analyzed with SEDFIT and SEDNTERP software.

UPLC-QTOF Analysis of IAA Products. We incubated sodium salt of IAA (2.5 mM; Sigma) (the salt was dissolved in 1× PBS, pH 7.0) with tES, free HRP, and tES-HRP (1 μM final concentration) at 37 °C for 1 h. The products of reacted IAA samples were characterized on UPLC-QTOF systems (1290 Infinity II LC + Agilent 6550B QTOF). Chromatographic separation was achieved with a linear gradient using mobile phase A (0.1% formic acid in water) and B (0.1% formic acid in acetonitrile) at a flow rate of 0.40 $mL \cdot min^{-1}$ on a Phenomenex Kinetex 2.6 μm XB-C18 100 Å 100 × 2.1 mm column maintained at 30 °C with a total run time of 20 min. The electrospray negative ionization (ESI−) mode was selected, and the mass/charge ratio was acquired in the 50−400 m/z range. Reference mass solution containing purine (119.04 m/z) and HP-0285 (302.00 m/z) dissolved in 95% acetonitrile/5% water/0.02% acetic acid was used for real-time TOF mass correction.

***In Vitro* Uptake Study.** The *in vitro* uptake of tES was studied with the triple-negative breast cancer cell line MDA-MB-231. A total of 15 $\times 10^6$ cells were cultured in Dulbecco's modified Eagle's medium (Sigma) supplemented with 10% fetal bovine serum (FBS) and 1% penicillin−streptomycin solution. The cultured cells were incubated with quantum dots (Qdot 605 ITK Carboxyl Quantum Dots, Thermo Fisher Scientific) encapsulated within tES for 8 h at room temperature, and the uptake of particles was evaluated using confocal microscopy (Olympus FV1000 TIRF) analysis after staining the cell lysosome with LAMP1 (C9091T, Lamp1 (D2D11) XP Rabbit mAb, Cell Signaling Technology) and the nucleus with DAPI (Prolong Gold Antifade Reagent with DAPI, Cell Signaling Technology). To study the mechanism underlying tES uptake, cells were treated with or without Dynasore hydrate (100 μM; Sigma-Aldrich) for 2 h at 37 °C, followed by their incubation with Alexa Fluor 647-labeled tES for 2 h at 37 °C. Following incubation, the cells were collected by treatment with trypsin−ethylenediaminetetraacetic acid (EDTA; Sigma-Aldrich) and the difference in the uptake efficiency between treated and untreated cells was evaluated using fluorescence-activated cell sorting (FACS; Cytoflex, Beckman Coulter).

***In Vitro* Bioorthogonal Catalysis.** The ability of tES-HRP to cleave the substrate IAA *in vitro* was evaluated in MDA-MB-231 and BT-549 cells. Briefly, MDA-MB-231 and BT-549 cells were seeded in 96-well plates at 1 × 10^4 cells/well and cultured overnight. The following day, media were changed to Opti-MEM and cells were assigned to one of the following treatment groups: (1) negative control (no treatment), (2) tES (500 μM), (3) tES-HRP (500 μM), (4) free HRP (equivalent to 500 μM tES-HRP) for overnight (all different treatments were incubated in 37 °C with 20 mM of HEPES

https://doi.org/10.1021/acsnano.1c11560
ACS Nano 2022, 16, 10292−10301

for 15 min before adding to the cells). The media were replaced with DMEM 12 h post-treatment, and 1 mM IAA was added to all the groups. The cells were incubated for 5 h at 37 °C, and cell viability was measured using CellTiter-Glo Luminescent Cell Viability Assay (Promega).

For the apoptosis study, 3×10^5 MDA-MB-231 cells were seeded in 6-well plates and the same protocol as cytotoxicity assay was performed. Five hours after adding the IAA, the cells were trypsinized and washed 2 times with cold PBS. The apoptosis assay proceeded with annexin V-FITC and propidium iodide (PI) double staining methodology. Flow cytometry experiment was then conducted on stained cells to discover the early or late apoptosis.[28,31] All the *in vitro* experiments were performed in triplicates.

Generation of MDA-MB-231 Xenograft Mouse Model. All animal experiments were performed as per the institutional guidelines and following an approved protocol by IACUC. Female athymic nude mice (5−6 weeks old) were purchased from In Vivos, Singapore, and housed in animal house facilities of NUS with a 12 h light/dark cycle. The animals had free access to food and water. Mice were acclimatized for a week before the start of the experiment, and MDA-MB-231 cells (1×10^6 in 200 μL of DPBS and Matrigel 1:1 mixture) were injected subcutaneously into a mouse mammary fat pad. The tumors were allowed to grow up to a volume of 200−250 mm^3 before the start of the treatment.

***In Vivo* Bioorthogonal Catalysis.** Following the previously established methodology for solid tumor treatment,[42,43] MDA-MB-231 xenograft-bearing mice were intratumorally injected with saline, empty tES, free HRP, or tES-HRP (400 $mg \cdot kg^{-1}$ body weight of each test agent; n = 8 per group), followed by an intraperitoneal administration of the prodrug IAA at 200 $mg \cdot kg^{-1}$ concentration every other day (a total of five injections). Body weight and animal behavior were monitored every other day until the treatment end. Tumor volume was measured thrice a week using a vernier calliper, and measurements were independently verified by a researcher blinded to treatment arm. Following the treatment completion, animals were sacrificed and the tumors excised.

Cleaved Caspase-3 Staining. The excised tumor tissues were embedded in optimum cutting temperature medium and tissue sections (10−20 μm) were obtained on a slide. For immunofluorescence staining, the slides were rehydrated in PBS for 5 min and subjected to antigen retrieval using 10 mM citrate buffer, pH 6.0 by boiling for 15−20 min in a water bath. The slides were washed thrice with PBS and tissues were permeabilized with 0.5% Triton X-100 in PBS for 10 min. The permeabilization buffer was rinsed-off and the nonspecific sites were blocked with 5% serum in PBST (PBS containing 0.1% Triton X-100). The blocking buffer was removed and the tissues were incubated overnight with primary cleaved caspase-3 antibody (cat. #9661; Cell Signaling Technology) at 4 °C. Nuclei were stained with DAPI. Following incubation, the slides were washed 3 times with TBST (Tris-buffered saline with 0.1% Triton X-100) and incubated with secondary antibody. The stained samples were imaged under confocal microscope (Olympus FV1000 TIRF).

***In Vivo* Biodistribution and Clearance Study.** Mice (n = 3) were intratumorally injected with saline, tES, free rLuc, or tES-rLuc (400 $mg \cdot kg^{-1}$ body weight), followed by an intraperitoneal injection of ViviRen *in vivo* Renilla Luciferase Substrate (0.3 mM) at 1, 3, 6, 12, 24, 48, and 72 h. The distribution of the particles was studied with the evaluation of bioluminescence using IVIS Spectrum.

***In Vivo* Toxicity Studies.** Mice (n = 3) were intratumorally injected with tES (400 $mg \cdot kg^{-1}$) for 5 consecutive days, followed by the analysis of blood biochemistry parameters such as liver function tests (albumin, alkaline phosphatase, alanine aminotransferase, and total bilirubin levels), kidney function tests (creatinine, total protein, and blood urea nitrogen levels), and hematological tests (white blood cell, red blood cell, hemoglobin, and hematocrit levels) on Abaxis VetScan VS2 Analyzer and hematology analyzer using comprehensive Diagnostic Profile Kit (catalog #500-0038, Alfamedic).

Statistical Analysis. All experiments were performed with at least three biological replicates. The data were presented as means ± standard error (SE). The Student's t-test and Mann−Whitney U test were used to identify differences between two groups as appropriate. Differences among three or more groups were assessed using one-way analysis of variance (ANOVA). P values less than 0.05 were considered statistically significant.

ASSOCIATED CONTENT

Supporting Information

The Supporting Information is available free of charge at https://pubs.acs.org/doi/10.1021/acsnano.1c11560.

Gene constructs; encapsulation and characterization of tES particles; structures and MS characterization of degradation products; prodrug conversion; *in vitro* cell uptake, cytotoxicity, and stability studies; *in vivo* characterization of tES in mice tumor model (Figures S1−S15) (PDF)

AUTHOR INFORMATION

Corresponding Author

Chester L. Drum − *Cardiovascular Research Institute, Department of Medicine, Yong Loo Lin School of Medicine, National University of Singapore, Singapore 119228, Singapore; Department of Medicine, Yong Loo Lin School of Medicine, National University of Singapore, Singapore 119228, Singapore; Department of Biochemistry, Yong Loo Lin School of Medicine, National University of Singapore, 117596, Singapore; Department of Surgery, Yong Loo Lin School of Medicine, National University of Singapore, Singapore 119228, Singapore;* orcid.org/0000-0001-6327-4584; Email: mdccld@nus.edu.sg

Authors

Samira Sadeghi − *Cardiovascular Research Institute, Department of Medicine, Yong Loo Lin School of Medicine, National University of Singapore, Singapore 119228, Singapore; Department of Medicine, Yong Loo Lin School of Medicine, National University of Singapore, Singapore 119228, Singapore; Genome Institute of Singapore (GIS), Agency for Science, Technology and Research (A*STAR), Singapore 138672, Singapore*

Nihar D. Masurkar − *Cardiovascular Research Institute, Department of Medicine, Yong Loo Lin School of Medicine, National University of Singapore, Singapore 119228, Singapore; Department of Medicine, Yong Loo Lin School of Medicine, National University of Singapore, Singapore 119228, Singapore*

Girish Vallerinteavide Mavelli − *Cardiovascular Research Institute, Department of Medicine, Yong Loo Lin School of Medicine, National University of Singapore, Singapore 119228, Singapore; Department of Medicine, Yong Loo Lin School of Medicine, National University of Singapore, Singapore 119228, Singapore*

Siddharth Deshpande − *Cardiovascular Research Institute, Department of Medicine, Yong Loo Lin School of Medicine, National University of Singapore, Singapore 119228, Singapore; Department of Medicine, Yong Loo Lin School of Medicine, National University of Singapore, Singapore 119228, Singapore; NUS Graduate School for Integrative Sciences and Engineering, National University of Singapore, Singapore 117456, Singapore*

Warren Kok Yong Tan − *Cardiovascular Research Institute, Department of Medicine, Yong Loo Lin School of Medicine, National University of Singapore, Singapore 119228, Singapore; Department of Medicine, Yong Loo Lin School of*

Medicine, National University of Singapore, Singapore 119228, Singapore; NUS Graduate School for Integrative Sciences and Engineering, National University of Singapore, Singapore 117456, Singapore

Sherman Yee − *Cardiovascular Research Institute, Department of Medicine, Yong Loo Lin School of Medicine, National University of Singapore, Singapore 119228, Singapore; Department of Medicine, Yong Loo Lin School of Medicine, National University of Singapore, Singapore 119228, Singapore*

Shin-Ae Kang − *Department of Biochemistry, Yong Loo Lin School of Medicine, National University of Singapore, 117596, Singapore*

Yoon-Pin Lim − *Department of Biochemistry, Yong Loo Lin School of Medicine, National University of Singapore, 117596, Singapore*

Edward Kai-Hua Chow − *Cancer Science Institute of Singapore, Yong Loo Lin School of Medicine, National University of Singapore, Singapore 117599, Singapore; Department of Pharmacology, Yong Loo Lin School of Medicine, National University of Singapore, Singapore 117597, Singapore*

Complete contact information is available at: https://pubs.acs.org/10.1021/acsnano.1c11560

Author Contributions

■S.S. and N.D.M. contributed equally to this work.

Funding

Agency for Science, Technology and Research (A2083c0055) Ministry of Health -Singapore > National Medical Research Council (CSAINV17nov012)

Notes

The authors declare no competing financial interest.

ACKNOWLEDGMENTS

We acknowledge funding from NMRC-Clinician Scientist Award, CSAINV17nov012 and A*STAR-AME, A2083c0055. Also, we thank Hossein Tabatabaeian for helping us in cytotoxicity assay and Gautam Sethi, Associate Professor, Department of Pharmacology for providing the BT549 cell line.

REFERENCES

(1) Zhang, X.; Huang, R.; Gopalakrishnan, S.; Cao-Milán, R.; Rotello, V. M. Bioorthogonal Nanozymes: Progress Towards Therapeutic Applications. *Trends in Chemistry* **2019**, *1*, 90−98.

(2) Sadeghi, S.; Lee, W. K.; Kong, S. N.; Shetty, A.; Drum, C. L. Oral Administration of Protein Nanoparticles: An Emerging Route to Disease Treatment. *Pharmacol. Res.* **2020**, *158*, 104685.

(3) van de L'Isle, M. O.; Ortega-Liebana, M. C.; Unciti-Broceta, A. Transition Metal Catalysts for the Bioorthogonal Synthesis of Bioactive Agents. *Curr. Opin. Chem. Biol.* **2021**, *61*, 32−42.

(4) Beltran-Torres, M.; et al. Comparative Studies of Structures and Peroxidase-Like Activities of Copper (II) and Iron (III) Complexes with an EDTA-Based Phenylene-Macrocycle and Its Acyclic Analogue. *ACS Omega* **2019**, *4*, 22487−22496.

(5) Lee, C. W.; Mubarak, M. Q. E.; Green, A. P.; De Visser, S. P. How Does Replacement of the Axial Histidine Ligand in Cytochrome c Peroxidase by Nδ-Methyl Histidine Affect Its Properties and Functions? A Computational Study. *International Journal of Molecular Sciences* **2020**, *21*, 7133.

(6) Berglund, G. I.; et al. The Catalytic Pathway of Horseradish Peroxidase at High Resolution. *Nature* **2002**, *417*, 463−468.

(7) Feng, L.; Dong, Z.; Tao, D.; Zhang, Y.; Liu, Z. The Acidic Tumor Microenvironment: a Target for Smart Cancer Nano-Theranostics. *National Science Review* **2018**, *5*, 269−286.

(8) Greco, O.; Folkes, L. K.; Wardman, P.; Tozer, G. M.; Dachs, G. U. Development of a Novel Enzyme/Prodrug Combination for Gene Therapy of Cancer: Horseradish Peroxidase/Indole-3-Acetic Acid. *Cancer Gene Ther.* **2000**, *7*, 1414−1420.

(9) Al-Bagmi, M. S.; et al. An Efficient Methodology for the Purification of Date Palm Peroxidase: Stability Comparison With Horseradish Peroxidase (HRP). *Saudi Journal of Biological Sciences* **2019**, *26*, 301−307.

(10) Voss, N.; et al. Targeting the Acidic Tumor Microenvironment: Unexpected Pro-Neoplastic Effects of Oral NaHCO3 Therapy in Murine Breast Tissue. *Cancers* **2020**, *12*, 891.

(11) Folkes, L. K.; Wardman, P. Oxidative Activation of Indole-3-Acetic Acids to Cytotoxic Species—a Potential New Role for Plant Auxins in Cancer Therapy. *Biochem. Pharmacol.* **2001**, *61*, 129−136.

(12) Devaraj, N. K. The Future of Bioorthogonal Chemistry. *ACS Central Science* **2018**, *4*, 952−959.

(13) Alonso-de Castro, S.; et al. Riboflavin As a Bioorthogonal Photocatalyst for the Activation of a Pt IV Prodrug. *Chemical Science* **2017**, *8*, 4619−4625.

(14) Dzijak, R.; et al. Structurally Redesigned Bioorthogonal Reagents for Mitochondria-Specific Prodrug Activation. *Jacs Au* **2021**, *1*, 23−30.

(15) Mirsky, I. A.; Diengott, D. Hypoglycemic Action of Indole-3-Acetic Acid By Mouth in Patients With Diabetes Mellitus. *Proceedings of the Society for Experimental Biology and Medicine* **1956**, *93*, 109−110.

(16) Ryšánek, K.; Vitek, V. Increased Excretion of 5-Hydroxy-Indole-Acetic Acid After the Administration of 3-Indole-Acetic Acid (heteroauxine). *Experientia* **1959**, *15*, 217−218.

(17) Spadiut, O.; Herwig, C. Production and Purification of the Multifunctional Enzyme Horseradish Peroxidase. *Pharmaceutical Bioprocessing* **2013**, *1*, 283.

(18) Tupper, J.; Stratford, M.; Hill, S.; Tozer, G.; Dachs, G. In Vivo Characterization of Horseradish Peroxidase With Indole-3-Acetic Acid and 5-Bromoindole-3-Acetic Acid for Gene Therapy of Cancer. *Cancer Gene Ther.* **2010**, *17*, 420−428.

(19) Deshpande, S.; et al. Thermostable Exoshells Fold and Stabilize Recombinant Proteins. *Nat. Commun.* **2017**, *8*, 1442.

(20) Landreh, M.; et al. Predicting the Shapes of Protein Complexes Through Collision Cross Section Measurements and Database Searches. *Anal. Chem.* **2020**, *92*, 12297−12303.

(21) Sadeghi, S.; et al. A general Approach to Protein Folding Using Thermostable Exoshells. *Nat. Commun.* **2021**, *12*, 5720.

(22) Vallerinteavide Mavelli, G.; Sadeghi, S.; Vaidya, S. S.; Kong, S. N.; Drum, C. L. Nanoencapsulation as a General Solution for Lyophilization of Labile Substrates. *Pharmaceutics* **2021**, *13*, 1790.

(23) Bekdemir, A.; Stellacci, F. A Centrifugation-Based Physicochemical Characterization Method for the Interaction Between Proteins and Nanoparticles. *Nat. Commun.* **2016**, *7*, 13121.

(24) Mehn, D.; et al. Analytical Ultracentrifugation for Analysis of Doxorubicin Loaded Liposomes. *Int. J. Pharm.* **2017**, *523*, 320−326.

(25) Tan, S.; Gu, D.; Liu, H.; Liu, Q. Detection of a Single Enzyme Molecule Based on a Solid-State Nanopore Sensor. *Nanotechnology* **2016**, *27*, 155502.

(26) Krintel, C.; et al. L-Asp Is a Useful Tool in the Purification of the Ionotropic Glutamate receptor A2 ligand-Binding Domain. *FEBS journal* **2014**, *281*, 2422−2430.

(27) Stopford, W.; Turner, J.; Cappellini, D.; Brock, T. Bioaccessibility Testing of Cobalt Compounds. *Journal of Environmental Monitoring* **2003**, *5*, 675−680.

(28) Wang, F.; et al. A Biocompatible Heterogeneous MOF−Cu Catalyst for in Vivo Drug Synthesis in Targeted Subcellular Organelles. *Angew. Chem., Int. Ed.* **2019**, *58*, 6987−6992.

(29) Wang, F.; Zhang, Y.; Du, Z.; Ren, J.; Qu, X. Designed Heterogeneous Palladium Catalysts for Reversible Light-Controlled Bioorthogonal Catalysis in Living Cells. *Nat. Commun.* **2018**, *9*, 1209.

(30) Chen, J.; Li, K.; Shon, J. S. L.; Zimmerman, S. C. Single-Chain Nanoparticle Delivers a Partner Enzyme for Concurrent and Tandem Catalysis in Cells. *J. Am. Chem. Soc.* **2020**, *142*, 4565−4569.
(31) Li, B.; et al. A Bioorthogonal Nanosystem for Imaging and In Vivo Tumor Inhibition. *Biomaterials* **2017**, *138*, 57−68.
(32) Mooney, R.; Majid, A. A.; Batalla, J.; Annala, A. J.; Aboody, K. S. Cell-Mediated Enzyme Prodrug Cancer Therapies. *Adv. Drug Delivery Rev.* **2017**, *118*, 35−51.
(33) Zhang, J.; Kale, V.; Chen, M. Gene-Directed Enzyme Prodrug Therapy. *AAPS Journal* **2015**, *17*, 102−110.
(34) Giang, I.; Boland, E. L.; Poon, G. M. Prodrug Applications for Targeted Cancer Therapy. *AAPS Journal* **2014**, *16*, 899−913.
(35) de Melo, M.; Curi, T.; Miyasaka, C.; Palanch, A.; Curi, R. Effect of Indole Acetic Acid on Oxygen Metabolism in Cultured Rat Neutrophil. *General Pharmacology: The Vascular System* **1998**, *31*, 573−578.
(36) de Melo, M. P.; de Lima, T. M.; Pithon-Curi, T. C.; Curi, R. The Mechanism of Indole Acetic Acid Cytotoxicity. *Toxicol. Lett.* **2004**, *148*, 103−111.
(37) Kim, D.-S.; Jeon, S.-E.; Park, K.-C. Oxidation of Indole-3-Acetic Acid by Horseradish Peroxidase Induces Apoptosis in G361 Human Melanoma Cells. *Cellular Signalling* **2004**, *16*, 81−88.
(38) Wardman, P. Indole-3-Acetic Acids and Horseradish Peroxidase: a New Prodrug/Enzyme Combination for Targeted Cancer Therapy. *Curr. Pharm. Des.* **2002**, *8*, 1363.
(39) John, J.; Blogg, C.; Murray, F.; Schwetz, B.; Gehring, P. Teratogenic Effects of The Plant Hormone Indole-3-Acetic Acid in Mice and Rats. *Teratology* **1979**, *19*, 321−326.
(40) Bahmani, B.; et al. Intratumoral Immunotherapy Using Platelet-Cloaked Nanoparticles Enhances Antitumor Immunity in Solid Tumors. *Nat. Commun.* **2021**, *12*, 1−12.
(41) Sheth, R. A.; et al. Assessment of Image-Guided Intratumoral Delivery of Immunotherapeutics in Patients with Cancer. *JAMA Network Open* **2020**, *3*, e207911−e207911.
(42) Hoop, M.; et al. Mobile Magnetic Nanocatalysts for Bioorthogonal Targeted Cancer Therapy. *Adv. Funct. Mater.* **2018**, *28*, 1705920.
(43) Shabat, D.; et al. In Vivo Activity in a Catalytic Antibody-Prodrug System: Antibody Catalyzed Etoposide Prodrug Activation for Selective Chemotherapy. *Proc. Natl. Acad. Sci. U. S. A.* **2001**, *98*, 7528−7533.
(44) Porter, A. G.; Jänicke, R. U. Emerging Roles of Caspase-3 in Apoptosis. *Cell Death & Differentiation* **1999**, *6*, 99−104.

https://doi.org/10.1021/acsnano.1c11560
ACS Nano 2022, 16, 10292−10301